Beam Steering Approach for Speckle Characterization and Out-of-Plane Motion Estimation in Real Tissue

Hassan Rivaz, Richard Zellars, Gregory Hager, Gabor Fichtinger and Emad Boctor

***Abstract*—Out-of-plane motion in freehand 3D ultrasound can be estimated using the correlation of corresponding patches, leading to sensorless freehand 3D ultrasound systems. Previous work has shown that the motion estimation in a beef tissue is systematically underestimated by approximately 33% and that it can be improved to approximately 25% by limiting the correlation calculation to the fully developed speckle (FDS) patches [1]. The improvement in the accuracy is limited because FDS patches are rare in real tissue. Here, we propose beam steering for detecting FDS patches and we show that it significantly improves speckle detection. We further experiment the effect of beam steering on out-of-plane motion estimation using ex-vivo beef liver and steak experiment. Without steered images, we find a 17% error in the liver experiment. Beam steering reduces the error to 9%, a significant improvement which is mainly due to enhanced FDS detection. Beef steak results are even more promising: 14.8% error without beam steering is reduced to 3.2% error.**

I. Introduction

Most common techniques for acquiring 3D ultrasound data are oscillating head probes and freehand 3D ultrasound. In oscillating head probes, a 1D ultrasound transducer is automatically swept inside the probe, enabling 3D image acquisition. In freehand 3D ultrasound, a position sensor is attached to an ordinary probe which is swept over the desire region by the clinician.

Freehand 3D ultrasound is inexpensive, works with the existing 2D probes, and allows arbitrary 3D volume acquisition. However, the need for the additional sensor makes it difficult to use. Sensorless volume reconstruction of freehand 3D ultrasound is possible using the information in the images themselves: out of plane motion estimation can be obtained from image correlation [2], which is the focus of this work, while in plane motion can be estimated through image registration [3], [4], [5].

Granular appearance of ultrasound images is the key factor in out-of-plane motion estimation. Each pixel in an ultrasound image is formed by the back-scattered echoes from an approximately ellipsoid called the resolution cell. The interference of scatterers in a resolution cell creates the granular appearance of the ultrasound image, called speckle. Although of random appearance, speckle pattern is identical if the same object is scanned from the same direction and under the same focusing and frequency. Speckle characterization is essential in many areas of quantitative ultrasound. In this work, it is a prerequisite for speckle-based distance estimation. We use low order moments to discriminate fully developed speckle (FDS) patches versus coherent speckle patches [6].

$$R = \mathrm{SNR} = \frac{\langle A^{v_r} \rangle}{\sqrt{\langle A^{2v_r} \rangle - \langle A^{v_r} \rangle^2}} \tag{1}$$

$$S = \mathrm{skewness} = \frac{\left\langle (A^{v_s} - \langle A^{v_s} \rangle)^3 \right\rangle}{(\langle A^{2v_s} \rangle - \langle A^{v_s} \rangle^2)^{\frac{3}{2}}} \tag{2}$$

where A is the amplitude of the ultrasound RF envelope in the analysis patch, v_r and v_s are the signal powers and $\langle \cdots \rangle$ denotes the mean. Here we use [7] $v_r = 2v_s = 1$. An elliptical discrimination function is calculated in the R-S plane by performing principal component analysis (PCA) on the data from simulated FDS patches [7]. A patch is then classified as FDS if its R-S duple falls inside this ellipse.

Having found FDS patches in two ultrasound images, the correlation between them is used for estimating the distance between the two images [1]. The R-S metric requires approximately 3500 pixels per patch (depending on the correlation of data [8]), but such large patches (which are rectangles) of FDS are unlikely to be found in real tissue because of its inhomogeneity [1]. Gee et al. [9] proposed a heuristic technique that is robust to the lack of FDS patches in the ultrasound image. This method allows the calculation of the elevational distance for all patches of the image, regardless of their level of coherency, by measuring the axial and lateral correlation of each patch. Since the behavior of coherent reflectors in the elevational direction can be different from their behavior in the axial and lateral directions, the performance of the method can decline depending on the level of anisotropy of the tissue.

In [10], we proposed a fast algorithm to find irregularly shaped FDS patches and showed that this algorithm finds significantly more FDS patches. Here, we propose using beam steering as another technique to increase the number of FDS patches found in the image. This is achieved by obtaining more data from a certain region of tissue, hence reducing the size of the analysis patch. Having found such small FDS patches, we further use the steered images for better out-of-plane (elevational) motion estimation.

H. Rivaz and G. Hager are with the Department of computer Science, R. Zellars is with the Department of Radiation Oncology and E. Boctor is with the Department of Radiology, Johns Hopkins University, Baltimore, USA.

G. Fichtinger is with the School of Computing, Queens University, Kingston, Canada.

Contact: rivaz@jhu.edu, eboctor@ieee.org

II. Speckle Characterization

Methods: We are looking for rectangular FDS patches using images acquired from the same location at different steering angles. The key idea is to combine data acquired from a certain region at different steering angles and therefore reducing the size of the analysis patch. Figure 1 shows two images acquired at 0 and θ steering angles. A rectangle patch in the left image is warped into a parallelogram and is shifted in the steered right image. The position of the parallelogram can be simply found as a function of θ, x and y. Therefore, samples n_X and n_Y from the steered image correspond to samples n_x and n_y from the non-steered image and

$$\begin{aligned} n_X &= n_x - \frac{v_{US}}{2\nu} \cdot \frac{n}{w} \cdot \sin(\theta) \cdot n_y \\ n_Y &= \frac{n_y}{\cos(\theta)} \end{aligned} \tag{3}$$

where $v_{US} = 1540000$mm/s is the speed of ultrasound in tissue, ν is the sampling frequency of the ultrasound machine, n is the total number of the A-lines and w is the width of image in mm. To find the correspondent of a patch, the correspondent of its four corners are found using these equations and applying nearest neighbor interpolation. The parallelogram connecting these four corners is the correspondent of the patch.

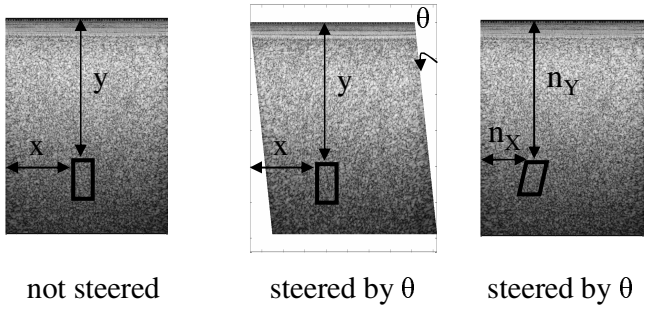

Fig. 1. **Corresponding patches in images acquired with different steering angles**. In the left, a patch is shown in the not-steered image. In the middle, the patch which corresponds to the same tissue is shown in the scan-converted steered image. In the right, the patch is shown in the raw steered image (not scan-converted).

Results: A Siemens Antares ultrasound machine (Issaquah, WA) with a sampling frequency of $\nu = 40$MHz is used to acquire RF data. 17 images of a FDS phantom are acquired at the 17 different steering angles of -5.5, -5, ... -2, 0, 2, 2.5 ...5.5 degrees, with increments of 0.5° except for -2° to 2° due to machine limitation. All the images are acquired from the same position by fixing the probe using a passive arm. The phantom is verified to be FDS using the R-S metrics with patches of size 3500 pixels in the non-steered image.

In the first experiment, the image with no steering is divided into rectangular patches (Figure 2 left). The patch size is varied from 500 to 3500 and the R-S test is applied to each patch by combining data from other steered images and without combining data. A 1D measure η for classification is obtained by first calculating the distance of the (R, S) point to the center of the FDS ellipse and then dividing it by the radius of the ellipse in the direction of the point: $\eta < 1$ and $\eta > 1$ represent the points inside (FDS) and outside (non-FDS) the ellipse respectively. Figure 2 right shows the results. Data from different steering angles are combined according to equation 3. The results show that exploiting the data acquired at two angles allows a reduction in the patch size by a factor of approximately two: $\bar{\eta}$ (mean of η) for patch size of 3500 pixels for individual angles is 0.87, which is equal to $\bar{\eta}$ at the patch size of 1750 for 2 angles. Including the 15 intermediate angles does not improve the results significantly, suggesting that the correlation between these images is high and they don't add new information.

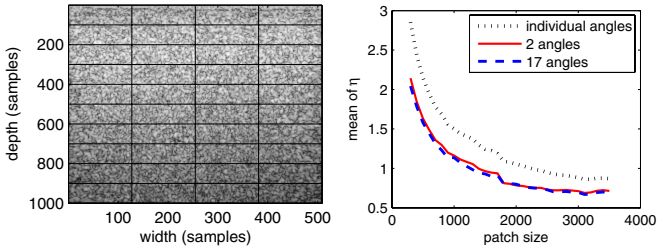

Fig. 2. **The effect of the patch size on the false rejection of the FDS patches**. In the left, subdivision of an image of the FDS phantom into patches is shown (patches are too large and are of size 100x127 for better illustration). In the right, the mean value of the η metric is shown for three cases: using each steering angle individually, combining two steering angle of -5.5° and 5.5° and combining all 17 steering angles. Since the phantom is FDS, small values of η are desirable.

In the second experiment, the patch size is fixed at 1750 pixels and the data from two steering angles are combined (to double the number of pixels to 3500). The $\bar{\eta}$ metric is calculated as a function of the difference in the steering angle of the two images (Figure 3). The $\bar{\eta}$ metric is also calculated for patches of size 3500 pixels in a single steering angle and is shown by an asterisk. The results show that at 11° separation between two images $\bar{\eta}$ is approximately equal to $\bar{\eta}$ for patch size of 3500 (the * in the figure). This suggests almost perfect decorrelated patches at 11° separation and is in accordance with the results of Figure 2.

Fig. 3. **The effect of the steering angle difference on the false rejection of the FDS patches**. The η value is calculated for sets containing 1750 pixels from each steering angle (total of 3500 pixels), and mean value of η as a function of the difference in the two steering angles is calculated. The mean of η is also calculated when each image is divided into patches of 3500 separately and is shown as a *.

III. Out-of-Plane Motion Estimation

The correlations are calculated using Pearsons linear correlation coefficient ρ

$$\rho(W,Z) = \frac{\Sigma w_i z_i - N\mu_w\mu_z}{\sqrt{\left(\Sigma w_i^2 - N\mu_w^2\right)\left(\Sigma z_i^2 - N\mu_z^2\right)}} \tag{4}$$

where w_i and z_i, $i = 1 \cdots N$, are the intensity values of each pixel in patches W and Z, N is the total number of pixels and μ_w and μ_y are the means of the intensity values of patches W and Z respectively.

To calibrate the rate of image decorrelation with out-of-plane motion, RF data of 3x51 parallel frames were acquired from a FDS phantom at an elevational distance of 0.05mm between consecutive images; three frames at each location with steering angles of -5.5, 0 and 5.5 degrees. The experimental setup is shown in Figure 4: the probe is moved with a micrometer with the accuracy of .001mm while the whole setup is secured on a rigid optical table. Calibration results showed that the decorrelation rate is not affected by beam steering.

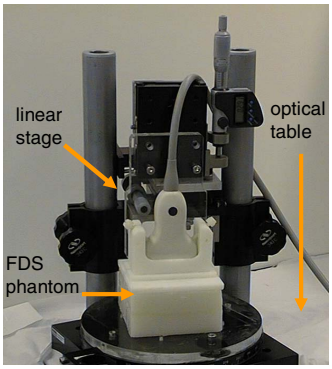

Fig. 4. **Calibration experimental setup**. Linear stage secured on an optical table for generating precise out-of-plane motion.

Out-of-plane motion estimation was performed on ex-vivo beef liver and steak data. For each tissue, 2x36 RF frames at an elevational distance of 0.2mm between consecutive frames were acquired using the setup shown in Figure 4; two images at each location with -5.5° and 5.5° steering angles. The distance between every two frames at a distance of $2 \times 0.2 = 0.4$mm is calculated using three approaches:

1) Only images at -5.5° are considered. Each image is divided into rectangular patches of size 3500 pixels and R-S speckle characterization is applied to each patch. The correlation coefficient is calculated for patches whose η is less than a threshold η_T [1] and the distance between patches is estimated using the decorrelation curves obtained from the FDS phantom.
2) Both of the images at -5.5° and 5.5° are considered. Speckle detection and correlation calculation is performed on each angle **separately** similar to the item 1 above using patch sizes of 3500 pixels and a threshold of η_T.
3) Both of the images at -5.5° and 5.5° are considered. The size of the patch window is decreased two fold and data from both angles are **combined** using equations 3 to end up with the same 3500 number of pixels in each patch. Speckles are classified like item 1 above using a threshold of η_T and image distances are calculated in patches with $\eta < \eta_T$ using the correlation calculated from all 3500 samples.

The procedure is repeated for all 36-2=34 pairs of images and the all of the estimated distances are stored. The mean and standard deviation of these values are shown in Figures 5 and 6 on the top for the liver and steak experiments. On the bottom, the average number of patches is shown as the threshold η_T is varied. Average number of patches is calculated by dividing the total number of distance measurements (associated with the patches with $\eta < \eta_T$) by 34. To estimate the rotation of the two images around the lateral and axial axes and the elevational motion the elevational distance between at least 3 non-collinear patches should be known.

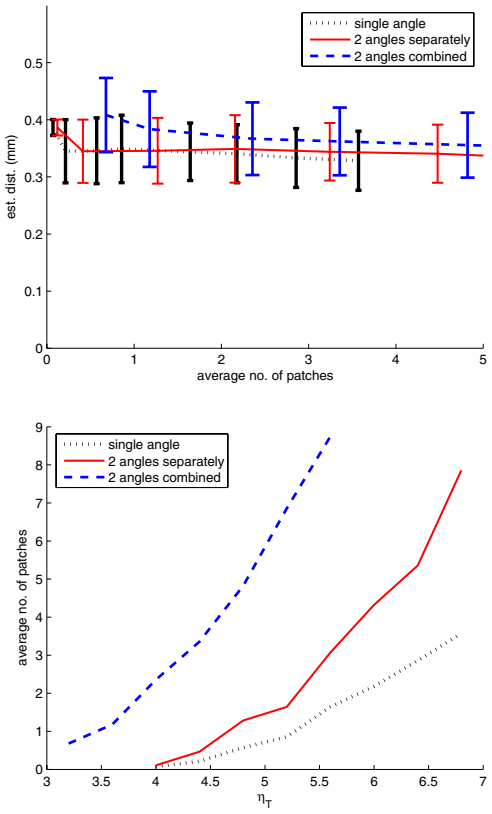

Fig. 5. **Ex-vivo beef liver experimental results**. On the top, mean and standard deviation of estimated distances between two frames that are 0.4mm apart are shown as the number of reference patches is changed by changing η_T. On the bottom, number of patches are shown as the threshold η_T is relaxed. All results are shown for the three described methods.

Considering the 0.4mm ground truth distance, method 3 is outperforming method 2 and method 2 is outperforming method 1. The errors for methods 1, 2 and 3 for the liver experiment at average number of patches of 3 is $\frac{0.4-0.332}{0.4} = 17\%$, $\frac{0.4-0.345}{0.4} = 13\%$ and $\frac{0.4-0.364}{0.4} = 9\%$ respectively. A comparison of errors of the three methods for the beef steak experiment is provided in Table I.

IV. Discussion and Conclusion

Results of Figure 2 show that the patch size can be reduced without increasing the false rejection of the R-S test. Figure 3 shows as the difference in the steering angle of two images increase, combining their information results in more reduction in the false rejection of the R-S test. At a steering angle difference of 11°, it seems that two images

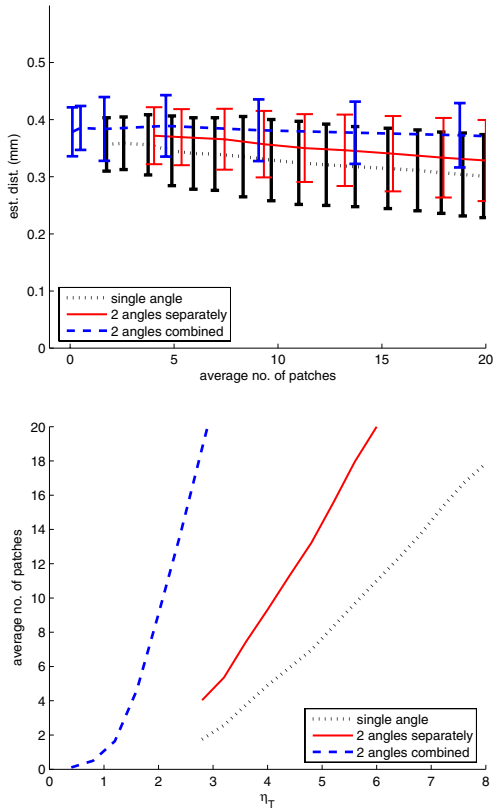

Fig. 6. **Ex-vivo beef steak experimental results**. On the top, mean and standard deviation of estimated distances between two frames that are 0.4mm apart are shown as the number of reference patches is changed by changing η_T. On the bottom, number of patches are shown as the threshold η_T is relaxed. All results are shown for the three described methods.

Avg. no. of patches	4	5	6	7	std
method 1	11.7%	13.8%	14.8%	15.0%	0.07mm
method 2	7.0%	7.5%	8.6%	8.5%	0.05mm
method 3	3.0%	3.0%	3.2%	3.7%	0.05mm

TABLE I
ERROR IN THE ESTIMATED DISTANCE IN THE BEEF STEAK. THE STANDARD DEVIATIONS FOR THE RANGE OF 4 TO 7 PATCHES ARE APPROXIMATELY CONSTANT WITHIN EACH METHOD AND ARE 0.07mm, 0.05mm AND O.05mm FOR METHOD 1, 2 AND 3 RESPECTIVELY.

are highly decorrelated since $\bar{\eta}$ value is almost equal to $\bar{\eta}$ value of a two times larger patch (asterisk in the figure). The improvement of motion estimation of approach 2 over approach 1 as discussed in Section III (Figure 5 and Figure 6) are due to the fact that having two images make it more likely to find FDS patches and therefore η_T can be reduced to find better patches. However, the improvement can be further increased by combining their information for reduced-size patch speckle detection, as we can see the smaller error of method 3 compared to method 2.

In summary, the significant improvement in out-of-plane motion estimation using image steering can be attributed to three factors. (1) Smaller patch size results in higher likelihood of finding uniform patches. (2) Boundaries appear fuzzy under an oblique US beam, which may lead to misclassification of the patch. Beam steering increases the chance of imaging boundary more perpendicularly, which reduces the likelihood of misclassification. (3) Averaging over more data increase the accuracy of estimation.

Out-of-plane motion estimation is only studied here for a fixed distance between two frames, 0.4mm. A study of accuracy as the distance varies gives insight for optimum frame selection [11], [12]. In freehand experiments the images are not parallel as they are in our experiments, and therefore the rotations between the images need to be found [13], [1], [9]. Recent work has studied a probabilistic approach on correlation based distance estimation [14] that result in enhanced out-of-plane motion estimation. We also showed before [10] that two-step meshing can significantly increase the number of FDS patches found in an ultrasound image of real tissue. Beam steering can be combined with these methods to achieve a higher accuracy sensorless freehand 3D ultrasound.

ACKNOWLEDGMENT

Authors would like to thank Siemens Medical especially Shelby Brunke. Supported by NSF EEC-9731748 and the Breast Cancer Research Foundation, USA.

REFERENCES

[1] P. Hassenpflug, R. Prager, G. Treece, and A. Gee, "Speckle classification for sensorless freehand 3-d ultrasound," *Ultrasound in Med. and Biol.*, vol. 31, pp. 1499–1508, November 2005.
[2] J. Chen, B. Fowlkes, P. Carson, and J. Rubin, "Determination of scan-plane motion using speckle decorrelation: theoretical considerations and initial test," *Imag. Sys. and Tech.*, vol. 8, pp. 38–44, 1997.
[3] G. Treece, R. Prager, A. Gee, C. Cash, and L. Berman, "Correction of probe pressure artifacts in freehand 3D ultrasound," *Medical Image Analysis*, vol. 6, pp. 199–215, 2002.
[4] B. Geiman, L. Bohs, M. Anderson, S. Breit, and T. G.E., "A novel interpolation strategy for estimating subsample speckle motion," *Pattern Recog. Letters*, vol. 45, pp. 1541–1552, 2002.
[5] R. Prager, A. Gee, G. Treece, C. Cash, and L. Berman, "Sensorless freehand 3-d ultrasound using regression of the echo intensity," *Ultrasound in Med. and Biol.*, vol. 29, pp. 437–446, 2003.
[6] R. Prager, A. Gee, G. Treece, and L. Berman, "Analysis of speckle in ultrasound images using fractional order statistics and the homodyned k-distribution," *Ultrasonics*, vol. 40, pp. 133–137, 2002.
[7] H. Rivaz, E. Boctor, and G. Fichtinger, "Ultrasound speckle detection using low order moments," *IEEE Int. Ultrasonics Symp.*, pp. 2092–2095, October 2006.
[8] V. Dutt and J. Greanleaf, "Speckle analysis using signal to noise ratios based on fractional order moments," *Ultrasonic Imag.*, vol. 17, pp. 251–268, 1995.
[9] A. Gee, R. Houdson, P. Hassenpflug, G. Treece, and R. Prager, "Sensorless freehand 3d ultrasound in real tissue: Speckle decorrelation without fully developed speckle," *Medical Image Analysis*, vol. 10, p. 137:149, April 2006.
[10] H. Rivaz, E. Boctor, and G. Fichtinger, "A robust meshing and calibration approach for sensorless freehand 3d ultrasound," *Proc. SPIE Medical Imaging*, vol. 6583, pp. 181–188, February 2007.
[11] W. Smith and A. Fenster, "Optimum scan spacing for three-dimensional ultrasound by speckle statistics," *Ultrasound in Med. and Biol.*, vol. 26, pp. 551–562, May 2000.
[12] W. Smith and A. Fenster, "Analysis of an image-based transducer tracking system for 3d ultrasound," *Proceedings of SPIE - The International Society for Optical Engineering*, vol. 5035, pp. 154–165, 2003.
[13] J. Housden, A. Gee, R. Prager, and G. Treece, "Rotational motion in sensorless freehand 3D ultrasound," *Univ. of Cambridge Tech. Rep.*, October 2007.
[14] C. Laporte and T. Arbel, "Probabilistic speckle decorrelation for 3d ultrasound," *Conference on Medical Image Computing and Computer Assisted Intervention*, November 2007.